

# Standard SANC modules for NLO QCD Radiative Corrections to Single-top Production <sup>1</sup>

D. Bardin\*, S. Bondarenko\*, P. Christova\*, L. Kalinovskaya\*,\*\*, V. Kolesnikov\*,  
W. von Schlippe<sup>‡</sup>, K. Yordanova<sup>†</sup>,

\* *Joint Institute for Nuclear Research, 141980 Dubna, Russia*

\*\*, *Higher Mathematics Department, The “Dubna” international University for Nature,  
Society, and Man, Dubna, 141980, Russia*

<sup>‡</sup> *PNPI, 188300 St. Petersburg, Russia*

<sup>†</sup> *Bishop Konstantin Preslavsky University, Shoumen, Bulgaria*

## Abstract

In this paper we present the results obtained with the newly created Standard SANC modules for calculation of the NLO QCD corrections to single top production processes in  $s$  and  $t$  channels at the partonic level, as well as top-decays. The main aim of these results is to prove the correct work of modules. A comprehensive comparison with results of the CompHEP system is given, where possible. These modules are intended to be used in Monte Carlo generators for single top production processes at the LHC. As in our recent paper, devoted to the electroweak corrections to these processes, we study the regularization of the top-legs associated infrared divergences with aid of the complex mass of the top quark. A comparison of QCD corrections with those computed by the conventional method is presented both for top production and decays. For  $s$  channel production we give an analytic proof of equivalence of the two methods in the limit of low top width.

**PACS:** 12.15.Lk, 13.40.Ks, 14.65.Ha, 12.38.-t.

## 1 Introduction

There is continued interest in precision calculations of single top quark production cross sections for the Tevatron and LHC (see *e.g.* [1] and references therein). This is motivated to a large extent by the fact that this process is the only way of measuring the CKM matrix element  $|V_{tb}|$  directly, providing a sensitive test of the 3-generation scheme of the Standard Model, and that it is an important background to various processes beyond the SM, including Higgs boson production.

Moreover, such events are already observed at the Tevatron experiments D0 [2, 3] and CDF [4, 5] and at the LHC [6]. There is a need to prepare software for precision analysis of the high statistics samples of single top quark events in future measurements at the LHC, running at 7 and 14 TeV.

Most of the theoretical work on single top production has been concerned with NLO QCD corrections (see *e.g.* [7], [8]), leading to the development of Monte Carlo generators, such as ZTOP [9], MC@NLO [10] or SingleTop [11], incorporated in the standard LHC tools.

---

<sup>1</sup>This work is partly supported by RFFI grant  $N^{\circ}10-02-01030-a$

In our previous paper [12] we have presented the calculation of the cross sections with one-loop electroweak corrections, regulating the infrared divergences (IRD) associated with the top-quark leg by introducing the width of the top quark.

In the present paper we extend that approach to the calculation of one-loop QCD corrections in the spirit of the complex-mass scheme [13]. To our knowledge there is no other work utilizing this approach to the IRD regularization among the many papers dealing with higher order QCD corrections to single top quark production, see *e.g.* [14] and references therein, as well as papers devoted to the complex-mass scheme itself, *e.g.* [15], [16].

This paper should be read together with [12], whose structure we have taken over here. In section 2 we recall the covariant amplitude for all processes  $t\bar{b}u\bar{d} \rightarrow 0$  and  $\bar{t}bu\bar{d} \rightarrow 0$  and show the conversions to the processes of  $t$  and  $\bar{t}$  decay and to  $s$  and  $t$  channel single top quark production, and point out the essential differences between the EW and QCD formulations of these processes. In section 3 we discuss in detail the regularization of single  $t$  and  $\bar{t}$  quark production in the conventional approach — with zero top quark width — and in the complex top quark mass approach. We present explicit formulas derived for both cases. In section 4 we present the results of numerical calculations which show the stability against variations of the soft-hard separation parameter and of the top quark width. Finally, in section 5 we present our conclusions and outlook to further work on single top quark production within the framework of SANC, aimed at the creation of an MC generator that simultaneously takes account of NLO EW and QCD corrections in the so-called 5F-scheme [8].

## 2 Covariant Amplitude

In this section we proceed in the spirit of the “multi-channel approach” developed in Refs. [17] and [18], and follow closely the presentation of our previous paper [12]. First, we consider annihilation into vacuum with all particles incoming.

### 2.1 All particles incoming

In QCD, there is no contribution from box diagrams such as those of [12] Figs. 1,2 which were appropriate for the EW case. Therefore in the present case we have a sum of two one-loop vertices instead of the two vacuum diagrams of [12]:

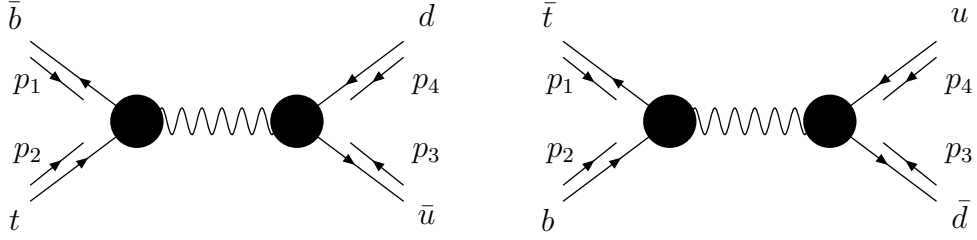


Figure 1: The  $\bar{t}b\bar{u}d \rightarrow 0$  and  $\bar{t}bu\bar{d} \rightarrow 0$  processes

The Covariant Amplitudes (CA) of Figs. 1 are characterized by four different structures and scalar Form Factors (FF) if the masses of the light quarks but not the  $b$  quark mass are neglected. A common expression for this CA in terms of four scalar form factors,  $\mathcal{F}_{LL,RL,LD,RD}(s,t)$ , was presented in Ref. [17]. We recall it here to introduce the notation:

$$\begin{aligned} \mathcal{A} = & i e^2 \frac{d_W(s)}{4} \left[ \gamma_\mu \gamma_+ \otimes \gamma_\mu \gamma_+ \mathcal{F}_{LL}(s,t) + \gamma_\mu \gamma_- \otimes \gamma_\mu \gamma_+ \mathcal{F}_{RL}(s,t) \right. \\ & \left. + \gamma_+ \otimes \gamma_\mu \gamma_+ (-iD_\mu) \mathcal{F}_{LD}(s,t) + \gamma_- \otimes \gamma_\mu \gamma_+ (-iD_\mu) \mathcal{F}_{RD}(s,t) \right], \end{aligned} \quad (1)$$

where

$$\gamma_\pm = (1 \pm \gamma_5), \quad D_\mu = (p_1 - p_2)_\mu. \quad (2)$$

4-momentum conservation reads

$$p_1 + p_2 + p_3 + p_4 = 0, \quad (3)$$

and the invariants are defined by

$$s = -(p_1 + p_2)^2, \quad t = -(p_2 + p_3)^2, \quad u = -(p_1 + p_3)^2, \quad (4)$$

with

$$s + t + u = m_t^2 + m_b^2. \quad (5)$$

Furthermore,

$$d_W(s) = \frac{V}{2s_W^2} \frac{1}{s - M_W^2 + iM_W\Gamma_W}, \quad (6)$$

where  $V = V_{tb}V_{ud}$  is the relevant product of CKM matrix elements. The scalar form factors  $\mathcal{F}$  are labeled according to their structures, see [17].

## 2.2 Conversion to top decay

The CA for the decay  $t(p_2) \rightarrow b(p_1) + u(p_3) + \bar{d}(p_4)$  is derived from the left Fig. 1 by the following 4-momentum replacement:

$$\begin{array}{ccc} p_1 & \rightarrow & -p_1, \\ p_2 & \rightarrow & p_2, \end{array} \quad \begin{array}{ccc} p_3 & \rightarrow & -p_3, \\ p_4 & \rightarrow & -p_4. \end{array}$$

For the decay  $\bar{t}(p_1) \rightarrow \bar{b}(p_2) + d(p_3) + \bar{u}(p_4)$  it is more transparent to make the replacement from the right Fig. 1:

$$\begin{array}{ccc} p_1 & \rightarrow & p_1, \\ p_2 & \rightarrow & -p_2, \end{array} \quad \begin{array}{ccc} p_3 & \rightarrow & -p_3, \\ p_4 & \rightarrow & -p_4. \end{array}$$

The corresponding two physical subprocess diagrams are those shown in Fig. 3,4 of [12].

## 2.3 Conversion to $s$ channel

The CA for the  $s$  channel single-top production processes  $\bar{u}(p_1) + d(p_2) \rightarrow b(p_3) + \bar{t}(p_4)$  is obtained from the left Fig. 1 by the replacement:

$$\begin{array}{ccc} p_1 & \rightarrow & -p_3, \\ p_2 & \rightarrow & -p_4, \end{array} \quad \begin{array}{ccc} p_3 & \rightarrow & p_1, \\ p_4 & \rightarrow & p_2, \end{array}$$

and for the processes  $\bar{d}(p_1) + u(p_2) \rightarrow t(p_3) + \bar{b}(p_4)$  from the right Fig. 1 by the conversion:

$$\begin{array}{ccc} p_1 & \rightarrow & -p_3, \\ p_2 & \rightarrow & -p_4, \end{array} \quad \begin{array}{ccc} p_3 & \rightarrow & p_1, \\ p_4 & \rightarrow & p_2. \end{array}$$

As a result we get the two physical subprocess diagrams shown in Fig. 5,6 of [12].

## 2.4 Conversion to $t$ channel processes

In the CAs for the  $t$  channel single-top production processes  $\bar{b}(p_1) + \bar{u}(p_2) \rightarrow \bar{d}(p_3) + \bar{t}(p_4)$  and  $\bar{b}(p_1) + d(p_2) \rightarrow u(p_3) + \bar{t}(p_4)$  it is convenient to make the replacement “in pairs”. From the left Fig. 1 one may perform two 4-momentum replacements:

$$\begin{array}{ccc} p_1 & \rightarrow & p_1, \\ p_2 & \rightarrow & -p_4, \\ p_3 & \rightarrow & p_2, \\ p_4 & \rightarrow & -p_3, \end{array} \quad \begin{array}{ccc} p_1 & \rightarrow & p_1, \\ p_2 & \rightarrow & -p_4, \\ p_3 & \rightarrow & -p_3, \\ p_4 & \rightarrow & p_2, \end{array}$$

which give rise to two different physical  $t$  channel processes as shown in Fig. 7 of [12].

For the processes  $b(p_1) + u(p_2) \rightarrow t(p_4) + d(p_3)$  and  $b(p_1) + \bar{d}(p_2) \rightarrow t(p_4) + \bar{u}(p_3)$ , the pair of replacements from the right Fig. 1,

$$\begin{array}{ccc} p_1 & \rightarrow & -p_4, \\ p_2 & \rightarrow & p_1, \\ p_3 & \rightarrow & -p_3, \\ p_4 & \rightarrow & p_2, \end{array} \quad \begin{array}{ccc} p_1 & \rightarrow & -p_4, \\ p_2 & \rightarrow & p_1, \\ p_3 & \rightarrow & p_2, \\ p_4 & \rightarrow & -p_3, \end{array}$$

gives the corresponding pair of symbolic diagrams for the two remaining  $t$  channel processes. They are shown in Fig. 8 of [12].

### 3 Process $ud \rightarrow tb$ at NLO QCD

#### 3.1 Notation and terminology

After conversion of the vacuum annihilation diagrams of Fig. 1 to the  $s$  channel, we will have two physical annihilation diagrams for both  $t$  and  $\bar{t}$  production (cf. symbolic diagrams in Fig. 5–6 of Ref. [12]). For our purpose it is sufficient to consider the top production NLO diagrams of Fig. 6 which, in turn, consist of ISR and FSR NLO contributions like the two fat vertices in diagrams in Fig. 1, standing for emission (and reabsorption) of a real (or virtual) gluon (cf. diagrams in Fig. 9,10 and 12 of Ref. [12]).

Since we are interested in the effects of the top quark width, the subject of our study will be only the symbolic FSR NLO diagram of Fig. 2. In the following, the label FSR will be assumed and omitted. It should be emphasized also that all the formulae of this Section refer to the limit  $m_b \rightarrow 0$ .

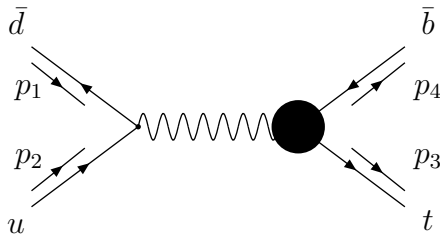


Figure 2: The FSR in the  $\bar{d}u \rightarrow t\bar{b}(g)$  processes

We will use the following common terminology:

- LO (or Born);
- NLO=Virtual + Real;
- Real=Soft + Hard;
- SV =Soft + Virtual (with 2→2 phase space);
- NLO=SV+HA (Hard Bremsstrahlung with 2→3 phase space).

#### 3.2 Conventional approach

In the conventional approach (stable particles) one introduces a soft–hard separation parameter

$$\bar{\omega} = 1 - \frac{s'_{\max}}{s}, \quad E_g^{\min} = \frac{\sqrt{s}}{2} \bar{\omega}, \quad (7)$$

with invariants  $s = M_{a,b}^2$  and  $s' = M_{c,d}^2$  for the radiative processes  $a + b \rightarrow c + d + g$ .

And for the total NLO cross sections we have

$$\sigma^{\text{NLO}}(s) = \sigma^{\text{SV}}(s, \bar{\omega}) + \sigma^{\text{HA}}(s, \bar{\omega}). \quad (8)$$

The infrared divergence cancels inside  $\sigma^{\text{SV}} = \sigma^{\text{S+V}}$  no matter how it is regularized (dimensionally or by a fictitious photon mass  $\lambda$ ), while the  $\bar{\omega}$  divergence cancels in the sum  $\sigma^{\text{NLO}} = \sigma^{\text{SV+HA}}$ , so that  $\sigma^{\text{NLO}}$  is finite.

At the end of this paragraph, we list the individual contributions.

Soft+Virtual:

$$\begin{aligned}\sigma^{\text{SV}}(s, \bar{\omega}) = & k_0 \left\{ \sigma^{\text{Born}}(s) \left[ -2 + (L_s - 2) \ln(\bar{\omega}) + \left( \frac{3}{4} - L_{t1} \right) L_b \right. \right. \\ & + \left( \frac{3}{2} \frac{m_t^2}{s_t} + \frac{5}{2} - 2L_{t1} \right) L_{t1} + \left( \frac{5}{2} \frac{m_t^2}{s_t} + \frac{3}{4} - 2L_{t1} \right) L_t + 2\text{Li}_2 \left( \frac{m_t^2}{s} \right) \Big] \\ & \left. + 2\text{Li}_2(1) - \frac{9}{4} K m_t^2 \frac{s_t}{s} (L_{t1} + L_t) \right\}. \quad (9)\end{aligned}$$

Hard:

$$\begin{aligned}\sigma^{\text{HA}}(s, \bar{\omega}) = & k_0 \left\{ \sigma^{\text{Born}}(s) \left[ \frac{9}{4} - \frac{m_t^2}{s_t} - (L_s - 2) \ln(\bar{\omega}) - \left( \frac{3}{4} - L_{t1} \right) L_b \right. \right. \\ & \left. \left. - \left( \frac{7}{2} - 2L_{t1} \right) L_{t1} - \left( \frac{3}{4} - L_{t1} \right) L_t - 2\text{Li}_2(1) \right] + \frac{1}{2} K (s_t + 2m_t^2 L_t) \right\}. \quad (10)\end{aligned}$$

Born or LO :

$$\sigma^{\text{Born}}(s) = \frac{1}{2} K \frac{s_t^2}{s^2} (2s + m_t^2). \quad (11)$$

Here and below:

$$\begin{aligned}k_0 &= \frac{\alpha_s C_f}{\pi}, \quad K = \frac{G_F^2 M_W^4 V^2}{6\pi [(s - M_W^2)^2 + M_W^2 \Gamma_W^2]}, \\ L_s &= 2 \ln \left( \frac{s_t}{m_t m_b} \right), \quad L_t = \ln \left( \frac{s}{m_t^2} \right), \quad L_b = \ln \left( \frac{s}{m_b^2} \right), \quad L_{t1} = \ln \left( 1 - \frac{m_t^2}{s} \right), \\ s_t &= s - m_t^2. \quad (12)\end{aligned}$$

In the NLO cross section all divergences, including  $b$  mass collinear divergences, cancel. The final expression is finite and very compact:

$$\begin{aligned}\sigma^{\text{NLO}}(s) = & k_0 \left\{ \sigma^{\text{Born}}(s) \left[ \frac{3}{4} - (L_t + 1) L_{t1} + 2\text{Li}_2 \left( \frac{m_t^2}{s} \right) \right] \right. \\ & \left. + \frac{1}{4} K \frac{m_t^2}{s^2} \left[ (5s_t (s + m_t^2) + 4m_t^2 s) L_t - 3s_t^2 (L_{t1} + 1) - 4m_t^2 s_t \right] \right\}. \quad (13)\end{aligned}$$

### 3.3 Infrared regularization by the complex top quark mass

The main aim of this paragraph is to show that the infrared regularization by the complex top quark mass leads exactly to the same final result, Eq. (13), though the partial expressions for SV and HA have a completely different form. For the introduction to the problem, we refer the reader to Section 3 of Ref. [12]. Here we again only list the individual contributions to the total cross sections.

Soft+Virtual:

$$\begin{aligned}\sigma^{\text{SV}}(s, \bar{\omega}, \Gamma_t) &= k_0 \left\{ \sigma^{\text{Born}}(s) \left[ -1 - (1 - L_s) \ln \left( \frac{\Gamma_t}{m_t} \right) - \ln(\bar{\omega}) \right. \right. \\ &\quad + \left( \frac{3}{4} - L_{t1} - L_t \right) L_b + \left( \frac{3}{4} - 3L_{t1} - \frac{1}{2}L_t \right) L_t + \left( \frac{5}{2} - 2L_{t1} \right) L_{t1} \\ &\quad \left. \left. + \text{Li}_2 \left( \frac{m_t^2}{s} \right) + 3\text{Li}_2(1) \right] - \frac{3}{4} K m_t^2 \frac{s_t^2}{s^2} (L_{t1} + L_t) \right\}. \quad (14)\end{aligned}$$

Hard:

$$\begin{aligned}\sigma^{\text{HA}}(s, \bar{\omega}, \Gamma_t) &= k_0 \left\{ \sigma^{\text{Born}}(s) \left[ \frac{5}{4} - \frac{m_t^2}{s_t} + (1 - L_s) \ln \left( \frac{\Gamma_t}{m_t} \right) + \ln(\bar{\omega}) \right. \right. \\ &\quad - \left( \frac{3}{4} - L_{t1} - L_t \right) L_b - \left( \frac{7}{2} - 2L_{t1} \right) L_{t1} \\ &\quad - \left( \frac{3}{4} - \frac{m_t^2}{s_t} - 2L_{t1} - \frac{1}{2}L_t \right) L_t + \text{Li}_2 \left( \frac{m_t^2}{s} \right) - 3\text{Li}_2(1) \left. \right] \\ &\quad \left. + \frac{1}{2} K (s_t + 2m_t^2 L_t) \right\}. \quad (15)\end{aligned}$$

We note the presence of two regularization parameters:  $\bar{\omega}$  is due to conventional treatment of infrared divergences associated with  $b$  quark legs, and  $\ln(\Gamma_t/m_t)$  is a new regularization parameter associated with the  $t$  quark leg, whose infrared divergence is regularized by its width. The individual (SV and HA contributions) have completely different form, but they sum up to exactly the same finite NLO expression (13) in which all three types of divergent terms ( $\ln(\Gamma_t/m_t)$ ,  $\ln(\bar{\omega})$ ,  $\ln(m_b)$ ) have canceled.

### 3.4 Relevant AV functions

The virtual contributions (due to vertex, Fig. 10, and the counter-term, Fig. 9, of Ref. [12]) were computed using the standard Passarino-Veltman reduction [19]. The relevant  $C_0$  function

$$C_0(-m_t^2, -m_b^2, Q^2; \tilde{m}_t, 0, m_b), \quad (16)$$

with complex argument

$$\tilde{m}_t^2 = m_t^2 + \Delta_t, \quad \Delta_t = -im_t \Gamma_t, \quad (17)$$

is given by Eqs. (22)–(24) of [12] and its limit at  $m_b \rightarrow 0$  by Eqs. (25)–(26) of that paper. Below we present its real part double limit:  $m_b \rightarrow 0$  and  $\Gamma_t \rightarrow 0$ , which was used in the derivation of Eq. (14):

$$\begin{aligned}\Re C_0(-m_t^2, -m_b^2, -s; \tilde{m}_t, 0, m_b) &= \frac{1}{s_t} \left\{ \left[ \ln \left( \frac{\Gamma_t}{m_t} \right) - L_{t1} - L_t \right] (L_b + L_t + 2L_{t1}) \right. \\ &\quad \left. + L_{t1} L_t + \frac{1}{2} L_t^2 - \text{Li}_2 \left( 1 - \frac{m_t^2}{s} \right) + 4\text{Li}_2(1) \right\}, \quad (18)\end{aligned}$$

In the calculation of the counter-term, one meets the real part of the derivative of a  $B_0$  function:

$$\Re [B'_0(-m_t^2, 0, \tilde{m}_t)] = \frac{1}{m_t^2} \ln \left( \frac{\Gamma_t}{m_t} \right). \quad (19)$$

### 3.5 Differential in $s'$ hard gluon radiation

The hard gluon contributions, Eq. (10) and Eq. (15), were derived by 4-fold integration in the  $2 \rightarrow 3$  process phase space over three angular variables and over the invariant  $s'$ , which varies within the limits  $m_t^2 \leq s' \leq s'_{\max}$ . In this paragraph we present the  $s'$ -integrands for the two approaches under consideration.

#### 3.5.1 Conventional approach

In the conventional approach, the expression for  $\sigma^{\text{HA}}(s, s')$  is well known:

$$\sigma^{\text{HA}}(s, s') = k_0 \left\{ \sigma^{\text{Born}}(s)(2 - L_{s'}) \left( \frac{1}{s_t} - \frac{1}{s - s'} \right) - K \frac{s - s'}{s} \left( \frac{s'_t}{s'} - k_1 L_{s'} \right) \right\}, \quad (20)$$

where

$$k_1 = \frac{1}{2} \left( 1 + \frac{1}{2} \frac{m_t^2}{s} \right), \quad L_{s'} = 2 \ln \left( \frac{s'_t}{m_t m_b} \right), \quad s'_t = s' - m_t^2. \quad (21)$$

The  $\bar{\omega}$  divergent term  $1/(s - s')$  after integration over  $s'$  gives rise to  $\ln(\bar{\omega})$  terms in Eq. (10) which cancel the corresponding terms in Eq. (9).

#### 3.5.2 Infrared regularization by the complex top quark mass

The expression for  $\sigma^{\text{HA}}(s, s')$  is more complicated in this case:

$$\begin{aligned} \sigma^{\text{HA}}(s, s') = & k_0 \left\{ \sigma^{\text{Born}}(s) \left[ \frac{1}{s_t} - \frac{1}{s - s'} + \frac{k^+}{2} L'_{s'} - \frac{1}{s_t} L_{s'} \right. \right. \\ & \left. \left. - \frac{1}{2} (I_1(s') + I_2(s')) - \frac{m_t^2}{s_t} I_3(s') \right] - K \frac{s - s'}{s} \left( \frac{s'_t}{s'} - k_1 L_{s'} \right) \right\}. \quad (22) \end{aligned}$$

Here,

$$\begin{aligned} L'_{s'} &= L_{s'} - \ln \left( \frac{s'}{m_b^2} \right), \\ k^\pm &= \frac{1}{s - s' + i\gamma_t} \pm \frac{1}{s - s' - i\gamma_t}, \\ \gamma_t &= \Gamma_t m_t. \end{aligned} \quad (23)$$

The three non-trivial objects to be integrated are:

$$\begin{aligned} I_1(s') &= k^+ \Re(J_b^W(0, m_t, \sqrt{s'}, i\gamma_t)), \\ I_2(s') &= ik^- \Im(J_b^W(0, m_t, \sqrt{s'}, i\gamma_t)), \\ I_3(s') &= \frac{1}{\gamma_t} \Im(J_b^W(0, m_t, \sqrt{s'}, i\gamma_t)), \end{aligned} \quad (24)$$



where

$$J_b^W(0, m_t, \sqrt{s'}, i\gamma_t) = \ln \left( \frac{i\gamma_t s' + (s - s')m_t^2}{i\gamma_t s' + (s - s')s'} \right), \quad (25)$$

and “0” in the argument list stands for the limit  $m_b \rightarrow 0$ .

Taking the integrals

$$I_i(s) = \int_{m_t^2}^s I_i(s') ds', \quad i = 1, 2, 3, \quad (26)$$

we get

$$\begin{aligned} I_1(s) &= \ln \left( \frac{s}{m_t^2} \right) \left[ \ln \left( \frac{\Gamma_t^2}{m_t^2} \right) - 2 \ln \left( \frac{s_t}{m_t^2} \right) \right] \\ &\quad - \text{Li}_2 \left( \frac{-s_t}{m_t^2} \right) + 2 \text{Li}_2 \left( \frac{s_t}{s} \right) - \text{Li}_2 \left( 1 + \frac{s}{m_t^2} \right) + \frac{3}{2} \text{Li}_2(1), \\ I_2(s) &= -\text{Li}_2 \left( \frac{-s_t}{m_t^2} \right) + \text{Li}_2 \left( 1 + \frac{s}{m_t^2} \right) - \frac{3}{2} \text{Li}_2(1), \\ I_3(s) &= \frac{1}{m_t^2} \left[ -s_t \ln \left( \frac{\Gamma_t}{m_t} \right) + s_t \ln \left( \frac{-s_t}{m_t^2} \right) - m_t^2 \ln \left( \frac{s}{m_t^2} \right) \right]. \end{aligned} \quad (27)$$

Substituting Eqs. (27) into Eq. (22) we arrive at Eq. (15).

## 4 Numerical Results

In this section we present the **SANC** results for the cross sections of the single top quark production processes and for the top quark decays. The tree level contributions, both Born and single real gluon emission, are compared with **CompHEP** versions v.4.4.3 [20] and v.4.5.1 [21]. All numerical results for this section were produced with the standard **SANC** INPUT working in the  $\alpha(0)$  EW scheme.

The **SANC** input parameters set:

$$\begin{aligned}
G_F &= 1.16637 \times 10^{-5} \text{ GeV}^{-2}, & \alpha_s &= 0.107 \\
\alpha(0) &= 1/137.035999, & \Gamma_w &= 2.141 \text{ GeV}, \\
M_W &= 80.403 \text{ GeV}, & \Gamma_z &= 2.4952 \text{ GeV}, \\
M_Z &= 91.1876 \text{ GeV}, & \Gamma_t &= 1.5517 \text{ GeV}, \\
M_H &= 120 \text{ GeV}, & m_d &= 83 \text{ MeV}, \\
m_u &= 62 \text{ MeV}, & m_s &= 215 \text{ MeV}, \\
m_c &= 1.5 \text{ GeV}, & m_b &= 4.7 \text{ GeV}, \\
m_t &= 174.2 \text{ GeV} \\
|V_{ud}| &= 1, & |V_{cs}| &= 1, \\
|V_{us}| &= 0, & |V_{cd}| &= 0, \\
|V_{tb}| &= 1.
\end{aligned} \tag{28}$$

Numbers used for the comparison with **CompHEP** for the decay channels were produced with **CompHEP** version 4.4.3 and with version v.4.5.1 for the production channels. For this comparison we use the standard **CompHEP** setup and the  $\alpha(0)$  EW scheme, however, we used  $\alpha_s = 0.12201$  ( $Q = M_Z$ ) and  $m_u = m_d = 66$  MeV. Moreover, in both codes we use the “fixed  $t$  width scheme”.

The structure, notation and terminology used of this Section are very similar to those of the corresponding Section 4 of Ref. [12]. We refer the reader to the paragraphs that follow Eq. (33) and do not repeat here Eqs. (34)–(35) and the surrounding text of the latter paper.

### 4.1 Decay channels $t \rightarrow b + u + \bar{d}$

#### 4.1.1 SANC–CompHEP comparison

In Table 1 we present results of the **SANC**–**CompHEP** comparison of radiative decay width  $\Gamma^{\text{hard}}$  in MeV for two cuts on the gluon energy:  $E_g \geq 5, 10$  GeV (in the top rest frame) and for two options:  $\Gamma_t = 0 (\neq 0)$  and six channels pid=19–24 for the case of **SANC** (pid=19,21,23 for  $\bar{t}$  decays, pid=20,22,24 for  $t$  decays).

The main aim of Table 1 is to demonstrate, for the first time, that there is good agreement between **SANC** and **CompHEP** not only for  $\Gamma_t = 0$ , but also for the  $\Gamma_t \neq 0$  options ( $\Gamma_t \neq 0$  always refers to the value in Eq. (28)).

#### 4.1.2 An internal SANC comparison

In **SANC** there are two modules for the computation of hard gluon bremsstrahlung processes: fully differential (5d), to be used in Monte Carlo simulations, and two dimensional (2d) in invariant variables  $s = -(p_t - p_b)^2$  and  $s' = -(p_u + p_d)^2$ , being analytically integrated over all angular variables. In order to check numerically the correctness of

$E_g$ , GeV	5		10	
	$\Gamma_t = 0$	$\Gamma_t \neq 0$	$\Gamma_t = 0$	$\Gamma_t \neq 0$
$t \rightarrow b + e^+ + \bar{\nu}_e + g$				
CompHEP	72.29(1)	71.80(2)	47.24(2)	47.13(2)
SANC , pid=19	72.28(1)	71.79(1)	47.20(1)	47.10(1)
SANC , pid=20	72.28(1)	71.79(1)	47.20(1)	47.10(1)
$t \rightarrow b + \mu^+ + \bar{\nu}_\mu + g$				
CompHEP	72.29(2)	71.80(2)	47.24(2)	47.13(2)
SANC , pid=21	72.28(1)	71.79(1)	47.20(1)	47.10(1)
SANC , pid=22	72.28(1)	71.79(1)	47.20(1)	47.10(1)
$t \rightarrow b + u + d + g$				
CompHEP	1296.9(6)	1295.6(5)	820.3(3)	819.7(3)
SANC , pid=23	1296.3(1)	1294.9(1)	819.8(1)	819.5(1)
SANC , pid=24	1296.3(1)	1294.9(1)	819.8(1)	819.5(1)

Table 1: SANC-CompHEP comparison of decay width  $\Gamma^{\text{hard}}$  in MeV in the  $\alpha$  scheme for two options:  $\Gamma_t = 0(\neq 0)$ ; and for six channels pid=19–24.

the analytic angular integration, we present Table 2 which shows the self-consistency of SANC calculations of the radiative contribution. Note that here  $E_g$  is the cut in the  $s'$  compound rest frame: this is why the numbers in Tables 1 and 2 are different.

$E_g$ , GeV	5		10	
	$\Gamma_t = 0$	$\Gamma_t \neq 0$	$\Gamma_t = 0$	$\Gamma_t \neq 0$
$t \rightarrow b + \mu^+ + \bar{\nu}_\mu + g$				
SANC-5d, pid=22	96.446(1)	94.459(1)	67.492(1)	67.085(1)
SANC-2s', pid=22	96.446(1)	94.459(1)	67.493(1)	67.085(1)
$t \rightarrow b + u + d + g$				
SANC-5d, pid=24	1245.6(1)	1239.6(1)	763.09(1)	761.87(1)
SANC-2s', pid=24	1245.6(1)	1239.6(1)	763.11(1)	761.88(1)

Table 2: SANC comparison of decay width  $\Gamma^{\text{Hard}}$  in MeV in the  $\alpha(0)$  scheme for two options:  $\Gamma_t = 0(\neq 0)$ ; two variants: 5d and 2s'; and for two channels pid=22 and 24.

#### 4.1.3 One-loop decay width

The numbers of this Section are produced with SANC setup (28) in the  $\alpha(0)$  EW parameterization scheme. We present results for two processes: pid=22 and 24.

- pid = 22. Process  $t \rightarrow b + \mu^+ + \bar{\nu}_\mu$

In Table 3 we show the lowest-order width  $\Gamma^{\text{Born}}$  as a function of the  $b$  quark mass. As is seen, the effect of a finite  $b$  quark mass is tiny. This justifies considering the limit  $m_b \rightarrow 0$ , in which the formulas are much shorter and which is convenient to study the validity of the KLN theorem in NLO approximation.

$m_b$ , GeV	4.7	1.0	0.1
$\Gamma^{\text{Born}}$ , GeV	0.149094(1)	0.149466(1)	0.149483(1)

Table 3: The total lowest-order width  $\Gamma^{\text{Born}}$  in GeV as function of  $m_b$ .

Table 4 demonstrates the stability of one-loop corrected quantities to the variation of the soft-hard separation parameter  $E_g$ .

$\Gamma_t = 0$			
$E_g$ , GeV	$10^{-1}$	$10^{-2}$	$10^{-3}$
$\Gamma^{1\text{-loop}}$	0.13651(1)	0.13652(1)	0.13651(1)
$\delta$ %	-8.440(1)	-8.437(2)	-8.439(9)
$\Gamma_t \neq 0$			
$\Gamma^{1\text{-loop}}$	0.13735(1)	0.13734(1)	0.13735(1)
$\delta$ %	-7.880(2)	-7.883(2)	-7.877(8)

Table 4: The total one-loop corrected width  $\Gamma^{1\text{-loop}}$  in GeV and relative one-loop correction  $\delta = (\Gamma^{1\text{-loop}} - \Gamma^{\text{Born}})/\Gamma^{1\text{-loop}}$  for  $E_g = 10^{-1}, 10^{-2}, 10^{-3}$  GeV and  $m_b=4.7$  GeV.

As is seen from Table 4, there is good  $E_g$  stability for  $E_g \leq 10^{-1}$  GeV. However, there is a rather big difference of the results for the one-loop corrected width  $\Gamma^{1\text{-loop}}$  and the relative QCD correction  $\delta$  of the partial decay width between the calculation with the  $\Gamma_t = 0$  and the  $\Gamma_t \neq 0$  options, where in the latter case we use the *fixed<sub>l</sub>* scheme defined in Ref. [12]. This difference gets smaller with formally decreasing  $\Gamma_t$  as Table 5 illustrates.

Table 5 demonstrates the two dimensional convergence of  $\Gamma^{1\text{-loop}}$  and  $\delta$  when both  $m_b$  and  $\Gamma_t$  go to zero. Note that with decreasing  $\Gamma_t$  the convergence in  $m_b$  improves.

$\Gamma^{1\text{-loop}}$ , GeV				
$\Gamma_t/10^N$ , $N$	0	1	2	$\Gamma_t = 0$
$m_b$ , GeV				
4.7	0.137345(2)	0.136594(2)	0.136518(3)	0.136515(3)
1.0	0.137919(2)	0.136840(2)	0.136726(3)	0.136717(3)
0.1	0.138479(2)	0.136900(2)	0.136738(3)	0.136723(5)
$\delta$ , %				
$\Gamma_t/10^N$ , $N$	0	1	2	$\Gamma_t = 0$
$m_b$ , GeV				
4.7	-7.881(1)	-8.384(1)	-8.436(2)	-8.437(2)
1.0	-7.726(1)	-8.448(1)	-8.523(2)	-8.530(2)
0.1	-7.362(1)	-8.418(1)	-8.526(2)	-8.537(3)

Table 5: The total one-loop corrected width  $\Gamma^{1\text{-loop}}$  in GeV and corresponding relative one-loop correction  $\delta$  in % as function of the  $b$  quark mass and of  $\Gamma_t$  with soft-hard separation parameter  $E_g = 10^{-2}$  GeV.

- pid = 24. Process  $t \rightarrow b + u + \bar{d}$

Here we present the corresponding set of Tables for the quark decay mode of the top quark.

The total lowest-order width (Table 6) also shows weak sensitivity to variations of the  $b$  quark mass.

$m_b$ , GeV	4.7	1.0	0.1
$\Gamma^{\text{Born}}$ , GeV	0.447284(1)	0.448399(1)	0.448451(1)

Table 6: The total lowest-order width  $\Gamma^{\text{Born}}$  in GeV as function of  $m_b$ .

The stability against variation of  $E_g$  is shown in Table 7.

$\Gamma_t = 0$			
$E_g$ , GeV	$10^{-1}$	$10^{-2}$	$10^{-3}$
$\Gamma^{1\text{-loop}}$	0.3594(1)	0.3581(1)	0.3584(4)
$\delta$ %	-19.65(1)	-19.94(1)	-19.89(6)
$\Gamma_t \neq 0$ , <i>fixed</i> <sub>1</sub>			
$\Gamma^{1\text{-loop}}$	0.3619(1)	0.3606(1)	0.3607(3)
$\delta$ %	-19.10(1)	-19.37(1)	-19.35(7)

Table 7: The total one-loop corrected width  $\Gamma^{1\text{-loop}}$  in GeV and relative one-loop correction  $\delta$  in % for  $E_g = 10^{-1}, 10^{-2}, 10^{-3}$  GeV and  $m_b=4.7$  GeV..

Similar conclusions as drawn after Table 4 are valid in this case. Finally, Table 8, showing the two dimensional limit, demonstrates similar behavior as Table 5 for the semi-leptonic top decay.

$\Gamma^{1\text{-loop}}$ , GeV				
$\Gamma_t/10^N$ , $N$	0	1	2	$\Gamma_t = 0$
$m_b$ , GeV				
4.7	0.36054(8)	0.35830(8)	0.35808(8)	0.35812(6)
1.0	0.36210(8)	0.35890(8)	0.35863(8)	0.35870(6)
0.1	0.36380(8)	0.35898(8)	0.35854(8)	0.35861(7)
$\delta$ , %				
$\Gamma_t/10^N$ , $N$	0	1	2	$\Gamma_t = 0$
$m_b$ , GeV				
4.7	-19.39(2)	-19.89(2)	-19.94(2)	-19.94(1)
1.0	-19.25(2)	-19.96(2)	-20.02(2)	-20.00(1)
0.1	-18.88(2)	-19.95(2)	-20.05(2)	-20.03(2)

Table 8: The total one-loop corrected width  $\Gamma^{1\text{-loop}}$  in GeV and corresponding relative one-loop correction  $\delta$  in % for  $E_g = 10^{-2}$  GeV as function of the  $b$  quark mass and of  $\Gamma_t$ .

## 4.2 $s$ channel

Here we consider  $s$  channel processes:

- pid=25,  $\bar{d} + u \rightarrow \bar{b} + t$  and pid=26,  $\bar{u} + d \rightarrow \bar{t} + b$   
but it is sufficient to consider one channel, say pid=25.

### 4.2.1 SANC–CompHEP comparison

$\sqrt{\hat{s}}$ , GeV	200	1000	7000
$\Gamma_t = 0$			
CompHEP	0.72930(2)	1.6340(1)	0.071223(1)
SANC-4d	0.72927(1)	1.6341(1)	0.071229(1)
SANC-s'	0.72928(1)	1.6338(1)	0.071227(1)
$\Gamma_t \neq 0$			
CompHEP	0.72638(2)	1.6323(1)	0.070946(1)
SANC-4d	0.72636(1)	1.6322(1)	0.070942(1)
SANC-s'	0.72636(1)	1.6322(1)	0.070942(1)

Table 9: Comparison of the cross section  $\sigma^{\text{Hard}}(\sqrt{\hat{s}}, \Gamma_t)$  in pb for three cms energies and two width options  $\Gamma_t = 0(\neq 0)$ . for pid = 25, i.e. for process  $\bar{d} + u \rightarrow \bar{b} + t$ ; the  $E_g$  cut is equal to 2 GeV.

As is seen from Table 9, there is very good agreement of numbers obtained from SANC and CompHEP within the statistical errors for two considered width options and three cms energies. In this case, the two widths options agree well for all three energies.

### 4.2.2 One-loop corrections

The analogue of Tables 4–9 of Ref. [12] is now represented by one joint Table 10 showing the stability of one-loop corrected QCD cross sections  $\hat{\sigma}^{1\text{-loop}}$  and relative QCD RC  $\delta$  against variation of the soft-hard separation parameter,  $\bar{\omega}$ , and the difference between the two options:  $\Gamma_t = 0(\neq 0)$ .

As is seen, there is good  $\bar{\omega}$  stability in the interval  $\bar{\omega} = 10^{-5} \div 10^{-6}$ ; also, the subtracted quantities  $\hat{\sigma}^{\overline{\text{MS}}}$  and  $\delta^{\overline{\text{MS}}}$  for all three cms energies and for both width options,  $\Gamma_t = 0(\neq 0)$ , are seen to be independent of the light quark masses.

One can see that the difference between the two width options is of order of few per mille in absolute deviation, rapidly decreasing with increasing cms energy. We therefore conclude that one may use the usual infrared regularization for  $s$  channel processes as was the case for EW corrections, see text after Table 6 of Ref. [12].

In Table 11 we demonstrate two dimensional convergence of  $\hat{\sigma}_1^{\overline{\text{MS}}}$  and  $\delta^{\overline{\text{MS}}}$  when both  $m_b$  and  $\Gamma_t$  go to zero. Note that, similarly to top decay cases, with lowering of  $\Gamma_t$  the convergence in  $m_b$  improves.

The agreement of  $\hat{\sigma}_1^{\overline{\text{MS}}}$  and  $\delta^{\overline{\text{MS}}}$  in the double limit (numbers for  $\Gamma_t/10^4$  and  $\Gamma_t = 0$ ) illustrates our analytic considerations described in Section 3.

$\sqrt{s}$ , GeV	200		1000		7000	
$\sigma^{\text{Born}}$ , fb	308.09055(1)		105.97718(1)		2.2352950(1)	
$\bar{\omega}$	$10^{-5}$	$10^{-6}$	$10^{-5}$	$10^{-6}$	$10^{-5}$	$10^{-6}$
$\Gamma_t = 0, m_q$						
$\hat{\sigma}^{\text{1-loop}}$	-374.05(1)	-374.07(1)	0.36446(1)	364.46(1)	17.599(1)	17.599(1)
$\delta$ , %	-221.41(1)	-221.42(1)	243.90(1)	243.90(1)	687.34(1)	687.34(1)
$\hat{\sigma}^{\overline{\text{MS}}}$	525.34(1)	525.37(1)	0.17057(1)	170.57(1)	8.2097(1)	8.2097(1)
$\delta^{\overline{\text{MS}}}$ , %	70.51(1)	70.53(1)	60.95(1)	60.95(1)	267.28(1)	267.28(1)
$\Gamma_t = 0, m_q/10$						
$\hat{\sigma}^{\overline{\text{MS}}}$	525.34(1)	525.37(1)	0.17057(1)	170.57(1)	8.2097(1)	8.2097(1)
$\delta^{\overline{\text{MS}}}$ , %	70.51(1)	70.52(1)	60.95(1)	60.95(1)	267.27(1)	267.28(1)
$\Gamma_t \neq 0, m_q$						
$\sigma^{\text{1-loop}}$	-372.85(1)	-372.87(1)	0.36455(1)	364.55(1)	17.601(1)	17.601(1)
$\delta$ , %	-221.02(1)	-221.03(1)	243.99(1)	243.99(1)	687.40(1)	687.40(1)
$\hat{\sigma}^{\overline{\text{MS}}}$	526.54(1)	526.57(1)	0.17066(1)	170.66(1)	8.2111(1)	8.2111(1)
$\delta^{\overline{\text{MS}}}$ , %	70.90(1)	70.91(1)	61.03(1)	61.03(1)	267.34(1)	267.34(1)
$\Gamma_t \neq 0, m_q/10$						
$\hat{\sigma}^{\overline{\text{MS}}}$	526.54(1)	526.57(1)	0.17066(1)	170.66(1)	8.2111(1)	8.2111(1)
$\delta^{\overline{\text{MS}}}$ , %	70.90(1)	70.91(1)	61.03(1)	61.03(1)	267.34(1)	267.34(1)

Table 10: The total lowest-order cross section  $\sigma^{\text{Born}}$ , one-loop cross section  $\hat{\sigma}^{\text{1-loop}}$  and total one-loop corrected  $\overline{\text{MS}}$  subtracted quantities  $\hat{\sigma}^{\overline{\text{MS}}}$  and corresponding  $\delta$  and  $\delta^{\overline{\text{MS}}}$  in % at  $\omega = 10^{-5}, 10^{-6}$  for  $\sqrt{s} = 200, 1000, 7000$  GeV.

$\hat{\sigma}_1^{\overline{\text{MS}}}$ , pb				
$\Gamma_t/10^N, N$	0	2	4	$\Gamma_t = 0$
$m_b$ , GeV				
4.7	0.52654(1)	0.52530(1)	0.52534(1)	0.52534(1)
1.0	0.53099(1)	0.52783(1)	0.52776(1)	0.52778(1)
0.1	0.53386(1)	0.52791(1)	0.52784(1)	0.52784(1)
0.01	0.53656(1)	0.52793(1)	0.52783(1)	0.52785(1)
$\delta^{\overline{\text{MS}}}$ , %				
$\Gamma_t/10^N, N$	0	2	4	$\Gamma_t = 0$
$m_b$ , GeV				
4.7	70.90(1)	70.50(1)	70.52(1)	70.51(1)
1.0	69.65(1)	68.64(1)	68.62(1)	68.62(1)
0.1	70.44(1)	68.54(1)	68.52(1)	68.52(1)
0.01	71.30(1)	68.55(1)	68.52(1)	68.52(1)

Table 11: The total one-loop corrected  $\overline{\text{MS}}$  subtracted cross sections  $\hat{\sigma}^{\overline{\text{MS}}}$  in pb and corresponding relative one-loop correction  $\delta^{\overline{\text{MS}}}$  in % for  $\sqrt{s}=200$  GeV (at the parton level) and for  $\bar{\omega} = 10^{-5}$  as function of the  $b$  quark mass and of  $\Gamma_t$ .

### 4.3 $t$ channel

#### 4.3.1 SANC–CompHEP comparison

This is the most complicated case:  $t$  channel cross sections show up bad statistical convergence. For this comparison we use CompHEP v.4.5.1 and its setup, but with non-zero masses of the  $u$  and  $d$  quarks (accessed via  $bc \rightarrow ts\gamma$  channel). For the Tables of this subsection we used  $m_q = m_u = m_d = 66$  MeV and  $10m_q$ , i.e.  $m_u = m_d = 660$  MeV. The cut on the cms gluon energy was  $E_g \geq 2$  GeV, and  $\alpha_s = 0.12201$  ( $Q = M_Z$ ). As in [12], rows marked “SANC(S)” (“S”hort massive case) were computed retaining  $m_q$  or  $10m_q$  only in fermion propagators radiating a gluon, while “SANC(F)” (“F”ully massive case) means that light quark masses were kept everywhere.

- pid = 27: Process  $b + u \rightarrow d + t$

$\sqrt{\hat{s}}/\text{GeV}$	200	1000	7000
$\Gamma_t = 0, m_q$			
CompHEP	17.908(1)	415.04(6)	617.40(6)
SANC(S)	17.904(1)	416.39(1)	618.94(1)
$\Gamma_t \neq 0, m_q$			
CompHEP	17.761(1)	404.29(6)	574.02(6)
SANC(S)	17.759(1)	405.62(1)	575.61(1)
SANC(F)	17.760(1)	405.63(1)	575.62(1)
$\Gamma_t \neq 0, 10m_q$			
CompHEP	11.792(1)	286.79(7)	400.29(2)
SANC(F)	11.789(1)	287.08(1)	400.48(1)

Table 12: Comparison of the cross section  $\hat{\sigma}^{\text{hard}}(\sqrt{\hat{s}})$  in pb for the process  $b + u \rightarrow t + d$  for three cms energies; three options of four:  $(\Gamma_t = 0(\neq 0)) \otimes (m_q, 10m_q)$ .

- pid = 28: Process  $b + \bar{d} \rightarrow \bar{u} + t$

$\sqrt{\hat{s}}/\text{GeV}$	200	1000	7000
$\Gamma_t = 0, m_q$			
CompHEP	10.335(1)	388.74(7)	615.5(1)
SANC(S)	10.332(1)	389.87(1)	616.86(1)
$\Gamma_t \neq 0, m_q$			
CompHEP	10.245(1)	378.21(7)	572.0(1)
SANC(S)	10.241(1)	379.34(1)	573.58(1)
SANC(F)	10.241(1)	379.35(1)	573.59(1)
$\Gamma_t \neq 0, 10m_q$			
CompHEP	6.641(1)	266.75(2)	398.68(4)
SANC(F)	6.640(1)	266.83(1)	398.83(1)

Table 13: The same as Table 12, but for the process  $b + \bar{d} \rightarrow \bar{u} + t$ .

The results of Tables 12–13 are qualitatively the same and may be discussed together.



There is satisfactory agreement for all options only near the reaction threshold. At higher energies **SANC/CompHEP** agree poorly for the  $m_q$  option and much better for the  $10m_q$  option. This allows us to draw conclusions similar to those which were drawn at the discussion of the results of analogous Tables 10–11 of Ref. [12].

#### 4.3.2 One-loop QCD corrections

The numerical results for this subsection were again produced with the aim to demonstrate the stability of one-loop corrected QCD cross sections  $\sigma^{1\text{-loop}}$  and relative QCD RC  $\delta$  against variation of the soft-hard separator  $\bar{\omega}$  and to study the difference between the two options:  $\Gamma_t = 0(\neq 0)$ .

- pid = 27. Process  $b + u \rightarrow d + t$

Table 14 is the counterpart for QCD of the six Tables 12–17 of Ref. [12].

$\sqrt{s}$ , GeV	200		1000		7000	
$\sigma^{\text{Born}}$ , pb	7.3551153(1)		48.993407(2)		50.824228(2)	
$\bar{\omega}$	$10^{-5}$	$10^{-6}$	$10^{-5}$	$10^{-6}$	$10^{-5}$	$10^{-6}$
$\Gamma_t = 0, m_q$						
$\hat{\sigma}^{1\text{-loop}}$	-5.741(1)	-5.742(1)	43.67(1)	43.66(1)	50.57(2)	50.57(2)
$\delta$ , %	-178.06(1)	-178.07(1)	-10.90(2)	-10.88(3)	-0.50(3)	-0.48(3)
$\hat{\sigma}^{\overline{\text{MS}}}$	10.215(1)	10.215(1)	47.67(1)	47.67(1)	50.71(2)	50.72(2)
$\delta^{\overline{\text{MS}}}$ , %	38.88(1)	38.88(1)	-2.70(2)	-2.69(3)	-0.23(3)	-0.20(4)
$\Gamma_t = 0, m_q/10$						
$\hat{\sigma}^{\overline{\text{MS}}}$	10.212(1)	10.210(1)	47.66(2)	47.66(2)	50.71(2)	50.72(3)
$\delta^{\overline{\text{MS}}}$ , %	38.88(2)	38.86(2)	-2.73(4)	-2.72(4)	-0.22(5)	-0.21(6)
$\Gamma_t \neq 0, m_q$						
$\sigma^{1\text{-loop}}$	-5.573(1)	-5.574(1)	43.94(1)	43.95(1)	50.87(2)	50.86(2)
$\delta$ , %	-175.77(1)	-175.78(1)	-10.29(3)	-10.28(2)	0.097(29)	0.063(34)

Table 14: The total lowest-order cross section  $\sigma^{\text{Born}}$ , one-loop cross section  $\hat{\sigma}^{1\text{-loop}}$  and total one-loop corrected  $\overline{\text{MS}}$  subtracted quantities  $\hat{\sigma}^{\overline{\text{MS}}}$  (all in pb) and corresponding  $\delta$  and  $\delta^{\overline{\text{MS}}}$  in % for  $\bar{\omega} = 10^{-5}, 10^{-6}$  and  $\sqrt{s} = 200, 1000, 7000$  GeV.

Stability in  $\bar{\omega}$  is seen to hold in all considered variants;  $m_q$  independence is clearly seen for the  $\Gamma_t = 0$  option. However, contrary to EW corrections, the dependence on  $\Gamma_t$  itself for non-subtracted quantities (compare two  $\delta$  rows) is much more pronounced, varying from several % near the threshold to half a percent at higher energies. Since it is not known how to realize subtraction for  $\Gamma_t \neq 0$  option, this difference may be treated as a theoretical uncertainty of NLO calculations which is, however, much smaller than the estimate of NNLO contributions [22].

For  $t$  channel processes, we show only one-dimensional convergence in the limit  $\Gamma_t \rightarrow 0$  for  $\sqrt{s} = 200$  GeV where our NLO correction is unphysical ( $< -100\%$ ), see Table 15. (We recall, that in this case we do not have an analytic proof of convergence similar to the proof shown in Section 3 for the  $s$  channel). So, it should be considered as only a formal, numerical illustration of convergence.

$\sqrt{s} = 200 \text{ GeV}, \sigma^{\text{Born}} = 7.3551153(1) \text{ pb}$		
$\Gamma_t/10^N, N$	$\hat{\sigma}^{1\text{-loop}}, \text{ pb}$	$\delta, \%$
0	-5.5730(6)	-175.77(1)
2	-5.7392(6)	-178.03(1)
4	-5.7419(7)	-178.07(1)
$\Gamma_t = 0$	-5.7411(6)	-178.06(1)

Table 15: The total lowest-order cross section  $\sigma^{\text{Born}}$ , the total one-loop corrected  $\hat{\sigma}^{1\text{-loop}}$  in pb and corresponding  $\delta$  in % at  $\sqrt{s} = 200 \text{ GeV}$  and  $\Gamma_t/10^N, N = 0, 2, 4$ .

- pid = 28. Process  $b + \bar{d} \rightarrow \bar{u} + t$

Table 16 is the counterpart for QCD of the six Tables 18–22 of Ref. [12].

$\sqrt{s}, \text{ GeV}$	200		1000		7000	
$\sigma^{\text{Born}}, \text{ pb}$	4.49579065(2)		46.6869560(1)		50.72449(1)	
$\bar{\omega}$	$10^{-5}$	$10^{-6}$	$10^{-5}$	$10^{-6}$	$10^{-5}$	$10^{-6}$
$\Gamma_t = 0, m_q$						
$\hat{\sigma}^{1\text{-loop}}$	-3.2657(4)	-3.2666(6)	39.71(1)	39.70(1)	50.22(2)	50.22(2)
$\delta, \%$	-172.64(1)	-172.66(1)	-14.95(2)	-14.96(3)	-0.99(3)	-1.00(4)
$\hat{\sigma}^{\overline{\text{MS}}}$	6.5587(4)	6.5586(6)	45.29(1)	45.29(1)	50.53(2)	50.52(2)
$\delta^{\overline{\text{MS}}}, \%$	45.88(1)	45.88(1)	-2.98(2)	-2.99(3)	-0.38(3)	-0.39(4)
$\Gamma_t = 0, m_q/10$						
$\hat{\sigma}^{\overline{\text{MS}}}$	6.5564(7)	6.5553(9)	45.28(2)	45.28(2)	50.51(3)	50.53(3)
$\delta^{\overline{\text{MS}}}, \%$	45.91(2)	45.88(2)	-3.01(4)	-3.02(4)	-0.42(5)	-0.39(6)
$\Gamma_t \neq 0, m_q$						
$\hat{\sigma}^{1\text{-loop}}$	-3.1526(4)	-3.1532(5)	39.99(1)	39.99(1)	50.52(1)	50.51(2)
$\delta, \%$	-170.12(1)	-170.14(1)	-14.35(2)	-14.34(3)	-0.40(3)	-0.41(3)

Table 16: The same as Table 14 but for pid = 28. Process  $b + \bar{d} \rightarrow \bar{u} + t$ .

$\sqrt{s} = 200 \text{ GeV}, \sigma^{\text{Born}} = 4.495790646(3) \text{ pb}$		
$\Gamma_t/10^N, N$	$\sigma^{1\text{-loop}}$	$\delta$
0	-3.1526(4)	-170.12(1)
2	-3.2644(4)	-172.61(1)
4	-3.2661(5)	-172.65(1)
$\Gamma_t = 0$	-3.2657(4)	-172.64(1)

Table 17: The same as Table 15 but for pid = 28. Process  $b + \bar{d} \rightarrow \bar{u} + t$ .

From Tables 16–17 the same conclusions may be drawn as from Tables 14–15. We will not repeat them here.

## 5 Conclusions and Outlook

In two papers, this one and Ref. [12], we have described the implementation into the **SANC** framework of the complete one-loop QCD and EW calculations, including hard bremsstrahlung contributions, for the processes of top quark decays and of  $s$  and  $t$  channel production, the latter two at the partonic level. Within the **SANC** framework, we have created the standard FORM and FORTRAN modules, see, Ref.[23], compiled into a package `sanc_cc.v1.40` which may be downloaded from the **SANC** project homepages [24].

The essentially new aspect of these two papers is the study of regularisation of the top quark-photon and -gluon infrared divergences with aid of the complex mass of the top quark. A comparison of these NLO corrections computed within this approach with those computed by the conventional method showed a difference which is not negligible, though not exceeding  $\sim 1\%$  for both types of corrections and for three considered processes. Although, the introduction of the non-zero top width within the fixed width scheme violates gauge-invariance, it is numerically not so important being of the order  $\mathcal{O}(\Gamma_t/m_t)$ ; it restores in the limit  $\Gamma_t \rightarrow 0$ .

The emphasis of these papers is to be assured of the correctness of our results. We observe the independence of the form factors on gauge parameters, checked the stability of the result against variation of the soft-hard separation parameter  $\bar{\omega}$  and the independence of the  $\overline{\text{MS}}$  subtracted quantities off the initial quark masses which is crucial for calculations at the hadronic level.

As has become **SANC** standard, we have compared our numerical results with other independent calculations wherever possible. For the decay channels it was done in our previous papers (both EW [25] and QCD [26]), showing good agreement. As usual, the Born level and the hard gluon contributions of all three channels were checked against the **CompHEP** package. We found very good agreement for both  $\Gamma_t = 0 (\neq 0)$  options.

As far as the comparison of EWRC for the production processes is concerned, it was described in our previous paper Ref. [12] and we found no suitable results in the literature on QCD corrections at the partonic level.

As a first step toward comparison of QCD calculations at the hadronic level we performed a triple comparison of the LO total cross sections of  $s$  and  $t$  channel single top production computed by **SANC/CompHEP/MCFM** with the same set of PDF. We found a satisfactory agreement between **SANC** and **CompHEP** numbers. The comprehensive comparison of the results at the hadronic level is the subject of ongoing work and a further publication.

All the calculations were done using a combination of analytic and Monte Carlo integration methods which will make it easy to impose experimental cuts in future calculations for  $pp$  collisions at the hadronic level. The results presented in these two papers lay a solid base for future extensions of calculations for the single top production channels at the LHC with subsequent decay in the cascade (factorized) approximation (see e.g. [27]) which simultaneously take account of NLO EW and QCD corrections.

**Acknowledgements.** This work is partly supported by Russian Foundation for Basic Research grant  $N^\circ$  10-02-01030.

WvS is indebted to the directorate of the Dzhelapov Laboratory of Nuclear Problems, JINR, Dubna, for the hospitality extended to him during April 2011.

## References

- [1] W. Bernreuther, *J. Phys.* **G35** (2008) 083001, 0805.1333.
- [2] D0 Collaboration, V. M. Abazov *et al.*, *Phys. Rev. Lett.* **98** (2007) 181802, hep-ex/0612052.
- [3] D0 Collaboration, V. M. Abazov *et al.*, *Phys. Rev. Lett.* **103** (2009) 092001, 0903.0850.
- [4] CDF Collaboration, T. Aaltonen *et al.*, *Phys. Rev. Lett.* **101** (2008) 252001, 0809.2581.
- [5] CDF Collaboration, T. Aaltonen *et al.*, *Phys. Rev. Lett.* **103** (2009) 092002, 0903.0885.
- [6] CMS Collaboration, S. Chatrchyan *et al.*, 1106.3052.
- [7] B. W. Harris, E. Laenen, L. Phaf, Z. Sullivan, and S. Weinzierl, *Phys. Rev.* **D66** (2002) 054024, hep-ph/0207055.
- [8] J. M. Campbell, R. Frederix, F. Maltoni, and F. Tramontano, *Phys. Rev. Lett.* **102** (2009) 182003, 0903.0005.
- [9] Z. Sullivan, *Phys. Rev.* **D70** (2004) 114012, hep-ph/0408049.
- [10] S. Frixione, E. Laenen, P. Motylinski, and B. R. Webber, *JHEP* **03** (2006) 092, hep-ph/0512250.
- [11] E. E. Boos, V. E. Bunichev, L. V. Dudko, V. I. Savrin, and A. V. Sherstnev, *Phys. Atom. Nucl.* **69** (2006) 1317–1329.
- [12] D. Bardin, S. Bondarenko, L. Kalinovskaya, V. Kolesnikov, and W. von Schlippe, *Eur. Phys. J.* **C71** (2011) 1533, 1008.1859.
- [13] A. Denner, S. Dittmaier, M. Roth, and D. Wackeroth, *Nucl. Phys.* **B560** (1999) 33–65, hep-ph/9904472.
- [14] N. Kidonakis, *Phys. Rev.* **D83** (2011) 091503, 1103.2792.
- [15] A. Denner and S. Dittmaier, *Nucl. Phys. Proc. Suppl.* **160** (2006) 22–26, hep-ph/0605312.
- [16] S. Actis, G. Passarino, C. Sturm, and S. Uccirati, *Phys. Lett.* **B669** (2008) 62–68, 0809.1302.
- [17] A. Andonov *et al.*, *Comput. Phys. Commun.* **174** (2006) 481–517, hep-ph/0411186.
- [18] D. Bardin, S. Bondarenko, L. Kalinovskaya, G. Nanava, and L. Rumyantsev, *Eur. Phys. J.* **C52** (2007) 83–92, hep-ph/0702115.
- [19] G. Passarino and M. J. G. Veltman, *Nucl. Phys.* **B160** (1979) 151.
- [20] <http://comphep.sinp.msu.ru/>, v.4.4.3.

- [21] <http://comphep.sinp.msu.ru/>, v.4.5.1.
- [22] N. Kidonakis, 1109.3231.
- [23] A. Andonov *et al.*, *Comput. Phys. Commun.* **181** (2010) 305–312, 0812.4207.
- [24] Dubna — <http://sanc.jinr.ru>, CERN — <http://pcphsanc.cern.ch>.
- [25] A. Arbuzov *et al.*, *Eur. Phys. J.* **C51** (2007) 585–591, hep-ph/0703043.
- [26] A. Andonov *et al.*, *Phys. Part. Nucl. Lett.* **4** (2007) 451–460.
- [27] D. Bardin, S. Bondarenko, P. Christova, L. Kalinovskaya, V. Kolesnikov, *et al.*, *Phys.Part.Nucl.Lett.* **7** (2010) 72–79, 0903.1533.